J Nanopart Res (2013) 15:1879
DOI 10.1007/s11051-013-1879-8

RESEARCH PAPER

Improved photodynamic action of nanoparticles loaded with indium (III) phthalocyanine on MCF-7 breast cancer cells

Carlos Augusto Zanoni Souto · Klésia Pirola Madeira · Daniel Rettori · Mariana Ozello Baratti · Letícia Batista Azevedo Rangel · Daniel Razzo · André Romero da Silva

Received: 1 April 2013 / Accepted: 16 July 2013

Abstract Indium (III) phthalocyanine (InPc) was encapsulated into nanoparticles of PEGylated poly (D,L-lactide-co-glycolide) (PLGA-PEG) to improve the photobiological activity of the photosensitizer. The efficacy of nanoparticles loaded with InPc and their cellular uptake was investigated with MCF-7 breast tumor cells, and compared with the free InPc. The influence of photosensitizer (PS) concentration (1.8–7.5 μmol/L), incubation time (1–2 h), and laser power (10–100 mW) were studied on the photodynamic effect caused by the encapsulated and the free InPc. Nanoparticles with a size distribution ranging from 61 to 243 nm and with InPc entrapment efficiency of 72 ± 6 % were used in the experiments. Only the photodynamic effect of encapsulated InPc was dependent on PS concentration and laser power. The InPc-loaded nanoparticles were more efficient in reducing MCF-7 cell viability than the free PS. For a light dose of 7.5 J/cm^2 and laser power of 100 mW, the effectiveness of encapsulated InPc to reduce the viability was 34 ± 3 % while for free InPc was 60 ± 7 %. Confocal microscopy showed that InPc-loaded nanoparticles, as well as free InPc, were found throughout the cytosol. However, the nanoparticle aggregates and the aggregates of free PS were found in the cell periphery and outside of the cell. The nanoparticles aggregates were generated due to the particles concentration used in the experiment because of the small loading of the InPc while the low solubility of InPc caused the formation of aggregates of free PS in the culture medium. The participation of singlet oxygen in the photocytotoxic effect of InPc-loaded nanoparticles was corroborated by electron paramagnetic resonance experiments, and the encapsulation of photosensitizers reduced the photobleaching of InPc.

Keywords PLGA-PEG · Indium phthalocyanine · Nanoparticles · MCF-7 cells · Photodynamic therapy

C. A. Z. Souto · A. R. da Silva (✉)
Federal Institute of Espírito Santo, Campus Aracruz, Avenida Morobá, 248, Morobá, Aracruz, ES 29192-733, Brazil
e-mail: aromero@ifes.edu.br

K. P. Madeira
Biotechnology Program/RENORBIO, Health Sciences Center, Federal University of Espírito Santo, Vitoria, ES 29040-090, Brazil

D. Rettori
Department of Exact Sciences and Earth, Federal University of São Paulo, Diadema, SP 09972-270, Brazil

M. O. Baratti
Department of Cellular Biology, University of Campinas, Campinas, SP 13083-863, Brazil

L. B. A. Rangel
Department of Pharmaceutical Sciences, Federal University of Espírito Santo, Vitoria, ES 29040-090, Brazil

D. Razzo
Department of Physical Chemistry, Institute of Chemistry, University of Campinas, Campinas, SP 13083-970, Brazil

Published online: 03 August 2013

Introduction

Photodynamic therapy (PDT) is an important therapeutic option for treating oncology (O'Connor et al. 2009; Sharma et al. 2012; Triesscheijn et al. 2006) and non-oncology (Allison et al. 2008; Calzavara-Pinton et al. 2005; Qiang et al. 2006) diseases. This modality combines a photosensitizer, light and oxygen molecules (Juzeniene et al. 2006; Ochsner 1997). After administration of the photosensitizer, the diseased tissue is illuminated with visible light. The irradiation leads to excitation of the PS to a singlet electronic state (S_1), which can be deactivated to the triplet state (T_1) by non-radioactive processes (intersystem crossing) (Juzeniene et al. 2006). In this state, the PS can interact with oxygen molecules or other biomolecules that are present near the irradiated region, thus generating reactive species that can damage the neoplastic tissues (Bozzini et al. 2012; Juzeniene et al. 2006; Ochsner 1997).

Administration of the lipophilic PS is a challenge in PDT because of the poor solubility of the molecules in physiologically compatible solvent media (Korbelik et al. 2012). To overcome this problem, various delivery strategies have been studied so far to preserve the hydrophobic photosensitizer in the aqueous environment (Bechet et al. 2008; Konan et al. 2002; Korbelik et al. 2012). Indeed, the development of drug delivery systems such as liposomes, micelles, and nanoparticles could improve the unfavorable biodistribution of free PS (i.e., improvement of photosensitizer pharmacokinetic properties, better targeting of diseased tissues due to particle size using the enhanced permeability, and retention effect, association to serum proteins and specific activation of the PS through localized delivery of the PS) as well as avoidance of aggregation and loss of phototoxic activity/fluorescence which should result in a better therapeutic outcome (Acharya and Sahoo 2011; Maeda et al. 2000; Sekkat et al. 2012; Soares et al. 2011). Polymeric nanoparticles have been prominent among the other delivery systems because of their capacity to release drugs at an experimentally predetermined rate over a prolonged period of time; maintain drug concentration with therapeutically appropriate ranges in circulation and within tissues; protect drugs from hepatic inactivation, enzymatic degradation and rapid clearance in vivo, and due to their simple preparation methods (Kamaly et al. 2012; Mundargi et al. 2008). Since poly(lactide-co-glycolide) (PLGA) is the most widely used polymer in pharmaceutical products approved by the Food and Drug Administration (FDA) due to their biocompatibility and biodegradability, this polymer has a long safety record (Blander and Medzhitov 2006; Mundargi et al. 2008). Therefore, our group has been exploring PLGA to encapsulate photosensitizers (Silva et al. 2009, 2011).

Several works have shown the benefits of PEGylation across a broad range of polymer molecular architectures and macromolecular assemblies in increasing the circulation half-life of polymeric nanoparticles that facilitate more opportunities for the passage of nanoparticles from the systemic circulation into the disordered and permeable regions of tumor vasculature (Cruz et al. 2011; Gref et al. 1994; Jokerst et al. 2011). In addition, polyethylene glycol (PEG) has been clinically validated for many different applications, and is currently listed as "Generally Recognized as Safe" by the FDA. This makes the PEGylated polymer particularly attractive for use in the encapsulation of a hydrophobic PS (Knop et al. 2010).

Metallic phthalocyanines stand among the most promising photosensitizers due to their intense absorption in the "photodynamic window" (600–800 nm), long triplet lifetimes, and large singlet oxygen quantum yields (Garcia et al. 2011; O'Connor et al. 2009). Considering that several metallic phthalocyanines have been used in clinical and preclinical trials in oncology (Sekkat et al. 2012) and that the presence of In(III) in the core of the photosensitizer structure enhances the in vitro and in vivo photodynamic efficacy (Chen et al. 2005; Rosenfeld et al. 2006), we decided to study indium(III) phthalocyanine (InPc) as a photosensitizer. Unfortunately, the InPc has a strong hydrophobic character that promotes aggregation in high polarity media hindering their systemic administration and restricting clinical studies. However, the encapsulation of InPc in nanoparticles can solve this problem.

The aim of this study was to encapsulate InPc in PLGA-PEG nanoparticles to improve the photobiological activity of the photosensitizer. The photodynamic efficacy of nanoparticles loaded with InPc on MCF-7 human breast tumor cells was evaluated and compared with free InPc. The particles were characterized with respect to surface morphology, size, zeta potential, InPc loading, and entrapment efficiency.

The effects of incubation time, InPc concentration, and laser power were studied on the photocytotoxicity of encapsulated or free InPc. The degree of internalization of InPc-loaded nanoparticles and of free InPc into cells was evaluated by confocal microscopy and afterward quantified by fluorescence. The formation of singlet oxygen by the encapsulated and free photosensitizer was evaluated by electron paramagnetic resonance (EPR), and the influence of photobleaching on these results was studied.

Experimental

Materials

PLGA-PEG (Resomer RGP d 50105, 45 kDa PLGA + 5 kDa PEG) was purchased from Evonik Rohm GmbH (Darmstadt, Hessen, Germany). Indium(III) phthalocyanine chloride, chloroform, poly(vinyl alcohol) (PVA) (M_w 13–23 kDa, 89 % hydrolysis degree), 2,2,6,6-tetramethyl-4-piperidone (TEMP), 4-(1,1,3,3-tetramethylbutyl)phenyl-PEG (Triton® X-100), trypsin, ethylenediaminetetraacetic acid (EDTA), trypan blue, 2-amino-2-(hydroxymethyl)-1,3-propanediol (Trizma® Base), sodium pyruvate, penicillin, gentamicin, amphotericin B, phalloidin-tetramethylrhodamine B isothiocyanate (phalloidin-TRITC), and propidium iodide were purchased from Sigma Chemical Company (St. Louis, MO, USA). Dimethylsulfoxide (DMSO), ethanol, sodium chloride, potassium chloride, dibasic sodium phosphate, monobasic potassium phosphate and paraformaldehyde were obtained from Vetec Química Fina Ltda (Duque de Caxias, RJ, Brazil). RPMI 1640 medium and fetal bovine serum were purchased from Cultilab (Campinas, SP, Brazil). ProLong® Gold with 4′,6 diamidine-2-phenylindol (DAPI) was obtained from Invitrogen (São Paulo, SP, Brazil). The water used throughout the experiment was first bi-distilled and then deionized (Millipore). All other chemicals were of analytical grade and were used without further purification.

Nanoparticle preparation

The particles were prepared using the emulsion/evaporation technique (Jeffery et al. 1991). For this method, the dispersion of an immiscible organic solvent in an aqueous phase with high pressure vapor, such as dichloromethane, is necessary. However, InPc is not soluble in dichloromethane. Thus, experiments were performed to determine the best solvent to solubilize InPc for preparing the PLGA-PEG nanoparticles loaded with InPc. An absorbance measurement of the free InPc solution (1.0–5.0 μmol/L) was obtained in 1-methyl-2-pirrolidone (MP), ethyl acetate (EA), dimethylformamide (DMF), and dimethylsulfoxide (DMSO). Graphics of absorbance versus concentration were obtained using the InPc absorbance values at the maximum absorbance wavelength in each solvent (682 nm for MP, 683 nm for DMF, 686 nm for DMSO, and 683 nm for EA) to determine the absorptivity coefficient. The solvent with the highest absorptivity coefficient was chosen as the best solvent for InPc.

For nanoparticle preparation, 50 mg of PLGA-PEG were dissolved in 7.0 mL of dichloromethane and 0.30 mg of InPc was dissolved in 3 mL of MP. The percentage of 30 % (v:v) of MP in the organic phase was adequate to prevent InPc aggregation when the InPc solution was mixed to PLGA-PEG solution. The organic phase (InPc solution + PLGA-PEG solution) was added slowly to 50 mL of an aqueous solution of PVA (1.5 % m/v) and ethanol (5 % v/v), which was homogenized for 15 min at 24,000 rpm (UltraTurrax T25, IKA, Wilmington, NC, USA). Since PLGA-PEG is characterized by a low glass transition temperature (Tg) (30 °C) (Lochmann et al. 2010), the jacketed glass was connected to an ultrathermostatic bath that maintained the internal circulating water at 15 °C. The initial and final temperatures of the solution were 20 ± 1 and 26 ± 2 °C, respectively. The resulting emulsion was maintained in magnetic agitation for 24 h for evaporation of organic solvents. The particles were recovered by centrifugation at 64,000×g for 22 min at 19 °C (Beckman J2-21, Beckman Instruments, Fullerton, CA, USA), and washed 3 times with water to remove excess PVA and non-incorporated InPc. Then, particle suspensions containing mannitol (mannitol: particle mass ratio of 1:1) were frozen in liquid nitrogen and freeze-dried at 28 μmHg and—45 °C in a LioBras lyophilizer, model LIOTOP L101 (São Carlos, SP, Brazil) for 2 days. Three independent formulations were prepared using this method.

Particle morphology and mean size

The morphology of nanoparticles was ascertained by scanning electron microscopy (SEM; JSM-6360 LV, JEOL, Tokyo, Japan). Approximately 2 mg of lyophilized particles were dispersed in deionized water and a droplet of this aqueous suspension was placed directly onto a metallic stub. Samples air-dried over the stub were coated with Au using a MED 020 Bal-Tec coater (Balzers, Liechtenstein). The mean particle size was determined by dynamic light scattering using a NPA152 Zetatrac from Microtrac (York, PA, US).

Determination of InPc content in the nanoparticles

An amount of lyophilized InPc-loaded nanoparticles (2.0 mg) without mannitol was dissolved in MP (2.0 mL) (a good solvent for both PLGA-PEG and the InPc). The InPc was quantified by UV–Vis spectroscopy (Agilent Cary 50 Conc, Santa Clara, CA, USA) at 682 nm using an analytical curve obtained with ten different InPc concentrations. The PLGA-PEG polymer did not cause interference at the selected wavelength. InPc incorporation efficiency was calculated using Eqs. (1) and (2). The determinations were carried out in triplicate and their mean values are reported.

$$\text{InPc loading } (\%) = \frac{\text{mass of photosensitizer in particles}}{\text{mass of particles}} \times 100 \quad (1)$$

$$\text{Entrapment efficiency } (\%) = \frac{\text{InPc loading}}{\text{Theoretical InPc loading}} \times 100 \quad (2)$$

Zeta potential measurement of nanoparticles

The zeta potential of nanoparticles was measured using dynamic light scattering technology (NPA152 Zetatrac, Microtrac Instruments, York, US) joined with the interaction of random Brownian motion with driven electric field motion of particle suspensions. Typically, 3 mg of the lyophilized nanoparticles were dispersed in 10 mL of deionized water, followed by sonication for a period of 1 min. The measure was done two times for each preparation. The zeta potential values represent the mean ± standard deviation (SD) for three independent preparations of nanoparticles.

Cultivation of cancer cells

MCF-7 human breast tumor cells (Rio de Janeiro Cell Bank, Duque de Caxias, RJ) were cultured in an RPMI 1640 medium supplemented with 10 % fetal bovine serum, 1.0 mmol/L sodium pyruvate, 2.0 mmol/L L-glutamine, 14 U.I./mL penicillin, 10 μg/mL gentamicin, and 3.5 μg/mL amphotericin, being incubated at 37 °C in a humidified environment having 5.0 % CO_2 (Sanyo, Bensenville, Il). After confluence was reached, the cells were washed twice with a phosphate-buffered saline (PBS) solution (1.8 mmol/L KH_2PO_4, 10.1 mmol/L Na_2HPO_4, 136.9 mmol/L NaCl, 2.7 mmol/L KCl) and harvested with trypsin (0.25 % m/v)-EDTA (0.02 % m/v) solutions. They were seeded at a density of 1.5×10^5 cells/well in 96-wells plates and allowed to grow for 48 h.

Photocytotoxic activity of the encapsulated and free InPc

The photocytotoxic effect of encapsulated and free InPc on the viability of MCF-7 cells was determined by 3-(4,5-dimethyl-2-thiazolyl)-2,5-diphenyl-2H-tetrazolium bromide (MTT) assay. The culture medium was removed and 200 μL fresh RPMI medium, without fetal bovine serum and containing either InPc-loaded nanoparticles or free InPc, were added to each well of a 96-wells plate so that the irradiation of a well does not reach the neighboring wells containing photosensitizer solution. The irradiation of the wells was done in the laminar flow cabinet. For the experiments performed with free InPc, the phthalocyanine was solubilized in MP solution (0.18 % volume MP: volume RPMI). The final InPc extracellular concentration was 7.5 μmol/L. Then, the MCF-7 cells (1.5×10^5 cells/well) were incubated for 1–2 h at 37 °C. After the desired incubation time, the wells were washed with PBS solution and a fresh culture medium was added. Each well was irradiated with a light dose of 7.5 J/cm^2 using a laser diode INOVA 665 nm of Laserline (Amparo, SP, Brazil). This laser has a current selector, allowing us to work with different powers. A laser power of 60 mW was used for the experiments performed to determine the influence of incubation time of the free or

encapsulated InPc on cell viability. Immediately after irradiation, the culture medium was removed from the well and 15 μL of MTT solution (5.0 mg/mL) were incubated for 4 h with cells. After this period, 70 μL of sodium dodecyl sulfate solution (10 % m:v) in HCl 0.01 mol/L were incubated with cells to solubilize the formazan crystals. After 12 h, absorbance of the formazan was measured in 570 nm in each well using an ELISA plate reader (Bioclin MR-96-A, Belo Horizonte, MG, Brazil) to determine cellular viability. The absorbance of treated cells and the control (untreated cell) were used for determining the percentage of cell viability (Eq. 3).

$$\% \text{ cell viability} = \frac{\text{absorbance of treated cells}}{\text{absorbance of the control}} \times 100 \quad (3)$$

The photocytotoxicity of InPc-loaded nanoparticles and of the free InPc was also evaluated by varying: (i) InPc concentrations (1.8–7.5 μmol/L) and (ii) laser power (10–100 mW). All experiments were carried out in a dark room to prevent the influence of surrounding radiation on the photocytotoxic effect. Dark control toxicity was examined through wells containing only cells incubated with RPMI, or cells incubated with RPMI and InPc-loaded nanoparticles or with free InPc, or cells incubated with RPMI and 0.18 % MP, or cells incubated with RPMI and InPc-free nanoparticles. Light control toxicity was also examined through wells containing only cells incubated with RPMI and irradiated by the laser diode 665 nm (light), or cells incubated with RPMI and 0.18 % MP and irradiated by the laser, or cells incubated with RPMI and InPc-free nanoparticle and irradiated by laser diode. The equivalent concentration of PLGA-PEG nanoparticles loaded with InPc was used in the experiment performed with free InPc nanoparticle. The results presented are the mean ± SD of three independent replicates. Statistical analyses were carried out using the Student's *t* test with a significance level of $p < 0.05$.

Quantification of internalized InPc

The encapsulated and free InPc internalized in MCF-7 cells was quantified through the method described by Win et al. (Win and Feng 2005). MCF-7 cells were grown in a 12-wells plate at 37 °C for 48 h using an RPMI 1640 medium. After this period, the wells with cells were washed twice with a phosphate-buffered saline solution. Then 2.0 mL of culture medium containing InPc-loaded nanoparticles or free InPc (7.5 μmol/L) were added to each well. After 2 h of incubation, cells were washed three times with the culture medium to eliminate excess particles or free InPc that was not entrapped by the cells and harvested with trypsin-EDTA solution. The suspension was centrifuged at 500×*g* for 5 min and the cells were resuspended with 500 μL of Triton® X-100 solution (0.5 % m:v) in a sodium hydroxide solution (0.2 mol/L) to permeabilize the cellular membrane and expose the encapsulated and free InPc. Subsequently, 1.5 mL of MP were added to solubilize the encapsulated and free InPc. The InPc in the cell extracts was determined spectrofluorimetrically, based on a previously constructed analytical curve using a PerkinHelmer LS 55 fluorescence spectrometer (Waltham, MA, USA). The values presented are the mean ± SD of three independent replicates. Statistical analyses were carried out using the Student's *t* test with a significance level of $p < 0.05$.

Cellular localization of InPc using confocal microscopy

MCF-7 cells (7.5×10^5 cells/mL) were seeded in plastic Petri dishes (16 × 10 mm) containing a spherical slide (∅ = 13 mm) immersed in RPMI 1640 medium complemented with 10 % fetal bovine serum. The Petri dishes were then incubated at 37 °C and 5 % of CO_2 for 48 h. The culture medium was removed and 500 μL of RPMI medium containing InPc-loaded nanoparticles or free InPc (7.5 μmol/L) were added to each dish. After 2 h of incubation, the cells were rinsed twice with a phosphate-buffered saline solution to eliminate the encapsulated or free InPc which was not attached to the cellular culture. Then, the cells were fixed with 4 % (m/v) paraformaldehyde solution for 20 min at room temperature, rinsed three times with PBS, and the slide was removed from the Petri dish. A Triton® X-100 solution (0.2 % m:v) in Trizma-buffered saline (TBS) solution (150 mmol/L of NaCl and 50 mmol/L of Trizma® base) was added on the slide surface for 5 min to permeabilize the cells. The permeabilization was blocked by placing a solution of bovine albumin (3 % m:v) in PBS on the slide surface for 30 min at room temperature. Subsequently, 100 μL of phalloidin-TRITC were placed onto the slide for 30 min to visualize the cell cytoskeleton. The slides were washed twice with

PBS to eliminate residual phalloidin-TRICT and 100 μL of a ProLong® Gold solution, containing 4′,6-diamidine-2-phenylindol (DAPI) were added to stain the cell nucleus at room temperature. All experiments were carried out in a dark room to prevent photodegradation of the probes. The slides were examined under a Zeiss Confocal LSM 510 microscope (Carl Zeiss microimaging, Inc., Thornwood, NY) equipped with Argon ($\lambda_{ex} = 543$ nm) and Helium–Neon ($\lambda_{ex} = 633$ nm) lasers. Phalloidin-TRICT was excited at 543 nm and its fluorescence was selected with a BP 560–615 filter that passes radiation with wavelengths ranging from 560 to 615 nm. The InPc was excited at 633 nm and its fluorescent emission was selected using an LP650 filter that passes radiation with wavelengths higher than 650 nm. The DAPI was excited using a mercury lamp and no filter was used. Optical cross-sections were obtained with a gradual increase of 1.57 and 0.79 μm in depth to evaluate the InPc-loaded nanoparticles and free InPc distribution in the cells, respectively.

InPc-loaded nanoparticles were incubated for 2 h with only culture medium to evaluate if the nanoparticle could aggregate in the culture medium during the incubation time with MCF-7 cells. The experiment was also performed in water to evaluate if the culture medium could cause the aggregation of the particles. The same concentration of nanoparticle (1.28 mg/mL) incubated with MCF-7 cells was used in this experiment. The average size of nanoparticle and the percentage of particles with a certain average size were measured in determined period during the incubation time (2 h) using the light dynamic scattering. The same procedure was performed in the culture medium to measure the size and percentage of free InPc aggregates. In this case, the concentration of free InPc was the same used in the experiment of irradiation of the cells (7.5 μmol/L). After 2.0 h of incubation, a Tween® 20 solution (0.24 mmol/L) was added to the nanoparticle or the free InPc solutions and the size and percentage of particles were measured again.

EPR measurements for detection of singlet oxygen

Generation of singlet oxygen was detected by EPR spectroscopy using TEMP. The reaction between $^1O_2$ and TEMP generates a stable nitroxide radical 2,2,6,6-tetramethyl-4-piperidone-*N*-oxide (TEMPONE) that is detectable using EPR measurements (Lion et al 1976). Typically, TEMP solutions (50 mmol/L) in RPMI 1640 medium, containing InPc-loaded nanoparticles or free InPc (7.5 μmol/L), were added to a cylindrical glass cell and afterward irradiated with a light dose of 3.0–7.5 J/cm^2 and a laser power of 100 mW at room temperature (25 °C). The same irradiation system (a laser diode 665 nm) was used in this experiment. Because of the hydrophobicity of InPc, the free InPc stock solution was prepared in MP solvent. Thus, the EPR experiment with free InPc was performed in culture medium containing 0.18 % (v:v) of MP. EPR spectra were recorded with a JES-FR30 JEOL spectrometer using a rectangular cavity after the incident light dose. Experiments were also performed in the presence of 5.0 μmol/L of NaN_3 (singlet oxygen suppressor) and 0.24 mmol/L of Tween® 20 (non-ionic surfactant). For assessing if singlet oxygen is generated by encapsulated InPc or by InPc molecules that were released from nanoparticles into the culture medium, the nanoparticles were incubated for 30 min in the medium, after which, the medium was centrifuged (24,000×*g*, 30 min) and the supernatant was irradiated in the presence of TEMP using a light dose of 7.5 J/cm^2. Measurements were carried out at room temperature with the following instrument settings: microwave power: 4 mW; microwave frequency: 9.41 GHz; field modulation frequency: 100 kHz; field modulation amplitude: 1 G; time constant: 0.30 s; scan time: 120 s; number of scans: 1; field center: 3375 G; field width: 15 G. All experiments were carried out in a dark room to prevent the influence of surrounding radiation.

Free and encapsulated InPc photobleaching

Stock solutions of free InPc were prepared in MP due to the low solubility of the photosensitizer in water. To obtain the desired concentration of InPc in the photobleaching assays (5.0 μmol/L), aliquots of the stock solution were added to a photooxidation medium composed of PBS solution and Tween® 20 (0.24 mmol/L). The concentration of Tween® 20 was kept above its critical micelle concentration (0.04 mmol/L) to reduce the formation of free InPc aggregates. The final percentage of MP in the photooxidation medium was the same percentage used in the experiments performed with MCF-7 cells (0.18 % v/v). The photooxidation medium containing free InPc

solution were added to a quartz cuvette and irradiated with a light dose of 0.5–5.0 J/cm^2 at room temperature using a laser diode 665 nm. The experiments were performed using several laser powers (1–60 mW). The same conditions were used to irradiate the free InPc solutions (5.0 μmol/L) prepared using MP from dilution of stock solution. In this experiment, the irradiated solution contained only InPc and MP. The InPc absorbance was monitored from 550 to 800 nm after each incident light dose. Then, a graphic of relative absorbance intensity versus light dose was obtained at 682 nm for free InPc solution prepared in MP (without PBS solution and Tween® 20), and at 690 nm for the free InPc solution diluted in PBS solution containing Tween® 20. The relative absorbance intensity was obtained by dividing the InPc absorbance intensity after light dose by absorbance intensity before irradiation. This procedure was repeated for each laser power. Suspension of InPc-loaded nanoparticles (with InPc concentration of 5.0 μmol/L) in PBS solution with 0.24 mmol/L of Tween® 20 was also irradiated with the same incident light doses and laser powers used in the photobleaching assays of the free InPc. After the light dose, the absorbance spectrum of encapsulated InPc was measured from 550 to 800 nm and the graphic of relative absorbance intensity at 690 nm versus light doses was obtained. In order to conclude whether the encapsulation of InPc decreases the photobleaching of the photosensitizer, the suspension was centrifuged at 20,400×g for 20 min and the InPc-loaded nanoparticles were recovered and dissolved in MP for three particular situations: before the irradiation of the suspension, after the incident light dose of 5 J/cm^2 with a laser power of 60 mW and after the same light dose but with a laser power of 100 mW. Subsequently, the absorbance spectrum of InPc in MP was measured and compared before and after incident light dose. All experiments were carried out in a dark room to prevent the influence of surrounding radiation on InPc photodegradation.

Free InPc spectra were obtained in MP or in PBS solution containing Tween® 20 for evaluation of the monomeric state of the InPc before the irradiation period carried out in the photobleaching experiments. Absorbance measurements were also performed with and without Tween® 20 to evaluate the presence of nanoparticle aggregates during the experiment with the encapsulated InPc.

Results and discussion

Preparation and characterization of InPc-loaded nanoparticles

Figure 1a disclosed that MP was more efficient to solubilize the InPc compared with other studied solvents since the absorbance of free InPc was the highest in MP. The absorptivity coefficient for InPc in MP [$(1.8 \pm 0.1) \times 10^5$ L/mol cm] was 15 times higher than the smallest absorptivity obtained in AE [$(1.2 \pm 0.1) \times 10^4$ L/mol cm] and increased according to the following order of solvents: AE [$(1.2 \pm 0.1) \times 10^4$ L/mol cm] < DMSO [$(2.2 \pm 0.4) \times 10^4$ L/mol cm] < DMF [$(4.5 \pm 0.7) \times 10^4$ L/mol cm] < MP [$(1.8 \pm 0.1) \times 10^5$ L/mol cm]. Therefore, we decided to use MP to dissolve InPc to prepare the InPc-loaded PLGA-PEG nanoparticles.

Since InPc is not soluble in dichloromethane, we evaluated whether the mixture of InPc solution in MP with dichloromethane could cause changes in the InPc spectrum. Figure 1b shows that the ratio of 30 % (v:v) of MP with 70 % (v:v) of dichloromethane did not change the InPc spectrum after 15 min of mixture (time used for preparing the nanoparticles). The PLGA-PEG also did not change the InPc spectrum when the polymer was dissolved in the mixture of MP and dichloromethane, and it did not show absorbance from 300 to 800 nm (Fig. 1b, inset). The result revealed that this mixture of MP with dichloromethane (30 and 70 % respectively) is efficient for maintaining the monomeric state of InPc molecules evidenced by a sharp Q band, typical of a monomeric phthalocyanine complex (Stillman and Nyokong 1989). This is important because the aggregation decreases the photodynamic efficacy of photosensitizer. Therefore, this mixture was used to prepare the PLGA-PEG nanoparticles loaded with InPc.

The SEM image of nanoparticles (Fig. 2) shows that particle shapes are spherical and are relatively homogenous in size. Dynamic light scattering results show that the average particle size was (127 ± 8) nm, and the particle sizes distribution ranged from 61 to 243 nm, with 90 % of the nanoparticles smaller than 200 nm (images not shown). Particles smaller than 200 nm stay in the bloodstream longer due to the reduced recognition of these particles by the mononuclear phagocytic system (Bourdon et al. 2000; Hans and Lowman 2002; Konan et al. 2003a). They also

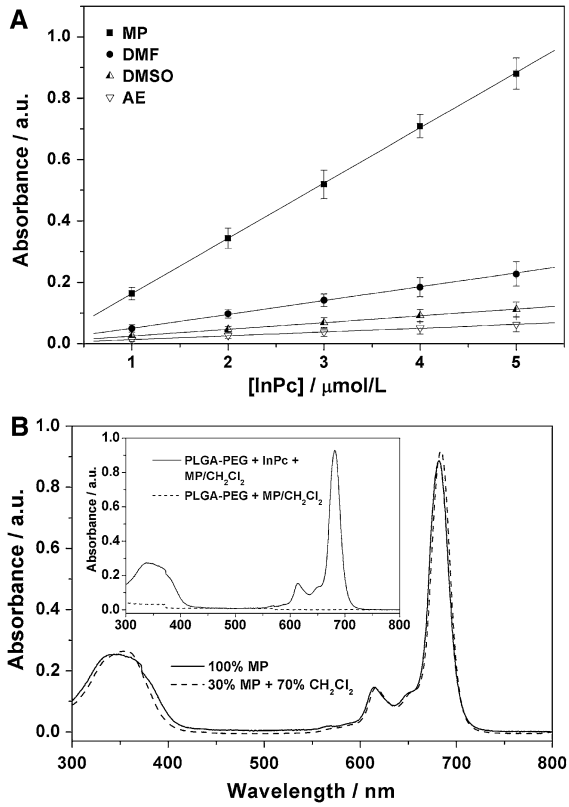

Fig. 1 **a** Absorbance intensity versus InPc concentration in several solvents. The absorbance values were determined at the InPc maximum absorbance wavelength for each solvent (682 nm for MP, 683 nm for DMF, 686 nm for DMSO and 683 nm for EA). The solvent with the highest absorptivity coefficient was chosen as the best solvent for InPc. **b** Absorbance spectra of InPc (5.0 μmol/L) dissolved in MP and in the mixture of 30 % (v:v) of MP with 70 % of dichloromethane. The PLGA-PEG also did not change the InPc spectrum (inset) when the polymer was dissolved in the mixture of MP and dichloromethane, and it did not show absorbance from 300 nm to 800 nm

interact more efficiently with cellular membranes (Win and Feng 2005). The PLGA-PEG nanoparticles exhibited an InPc entrapment efficiency of around (72 ± 6) %, a loading value of around (0.43 ± 0.04) % and a zeta potential of −33.9 ± 3 mV.

Viability of MCF-7 cells in action involving only InPc-free nanoparticles, light and MP

The photocytotoxic effect on the viability of MCF-7 cells after incubation and irradiation with InPc-free nanoparticles was not observed. This is consistent with PLGA-PEG biocompatibility. The light emitted by the laser and MP (0.18 % v:v) were also not cytotoxic to the cells (results not shown). Therefore, InPc-free nanoparticles, light and MP did not influence the results obtained for cell viability of MCF-7 cells incubated with InPc-loaded particles or the free InPc.

Effect of incubation time on phototoxicity

A significant decrease in cell viability was observed after a light dose of 7.5 J/cm^2 when the MCF-7 cells were incubated with InPc-loaded PLGA-PEG nanoparticles for 1 h since the viability decreased from (100 ± 5) % (number of control cells) to (44 ± 4) % (cells + nano/InPc + light) (Fig. 3). A similar decrease in cell viability was obtained when cells were incubated with InPc-loaded nanoparticles for 1.5 and 2 h and irradiated by the same light dose since viability was reduced to (49 ± 9) % and to (47 ± 10) %, respectively, suggesting the photodynamic effect was not changed after 1 h of incubation (Fig. 3).

The free InPc reduced cell viability from (100 ± 10) % (number of control cells) to (69 ± 6) % (cells + free InPc + light) only after 1.5 h of incubation and subsequent irradiation (Fig. 3). The increase in incubation time of 1.5–2 h did not have any significant effect on cell viability since viability was maintained at (69 ± 4) %, suggesting the photodynamic effect was not changed after the incubation time of 1.5 h (Fig. 3). Neither encapsulated InPc nor free InPc caused cytotoxic effects (without light) to MCF-7 cells under the same conditions (Fig. 3). Statistical analysis shown that the encapsulated InPc was more efficient than free InPc in

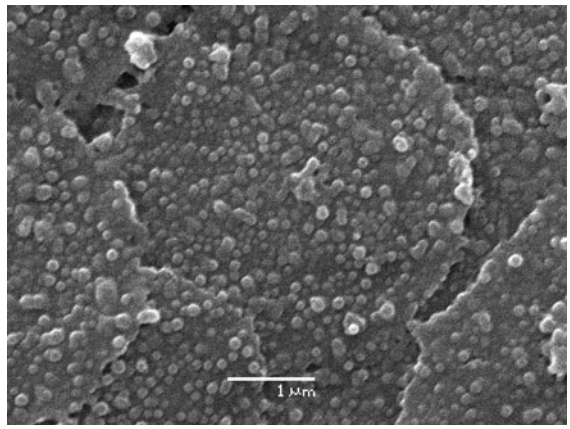

Fig. 2 SEM images of InPc-loaded PLGA-PEG nanoparticles, prepared by the emulsion/evaporation method using PVA as emulsifier

causing cellular death since less cell viability was obtained using InPc-loaded nanoparticles with 1 h [(44 ± 4) %], 1.5 h [(49 ± 9) %], or 2 h [(47 ± 10) %] of incubation and 7.5 μmol/L of InPc whether compared with the viability obtained using free InPc for 1 h [(92 ± 9) %], 1.5 h [(69 ± 6) %], or 2 h [(69 ± 4) %] of incubation (Fig. 3). It seems that encapsulated InPc was internalized faster than free InPc since the photocytotoxic effect was observed after an incubation time of 1 h for InPc encapsulated and after 1.5 h for free InPc. Since the reduction in cellular viability between 1.5 and 2 h was not significantly different for MCF-7 cells incubated with InPc-loaded nanoparticles, or with free InPc, after irradiation with a light dose of 7.5 J/cm^2 and laser power of 60 mW, an incubation time of 2 h was used for subsequent experiments.

Effect of InPc concentrations on phototoxicity

The increase in encapsulated InPc concentration from 1.8 to 7.5 μmol/L increased the photocytotoxicity of the nanoparticulate formulation since cell viability decreased from (100 ± 5) % (number of control cell) to (82 ± 3) % (number of cells + nano/InPc + light) for a concentration of 1.8 μmol/L, subsequently to (63 ± 3) % (number of cells + nano/InPc + light) for a concentration of 3.8 μmol/L and then to (47 ± 6) % (number of cells + nano/InPc + light) when the InPc concentration was 7.5 μmol/L (Fig. 4). However, free InPc only reduced cell viability from (100 ± 6) % (number control of cells) to (71 ± 8) % (number of cells + free InPc + light) when the InPc concentration was 7.5 μmol/L (Fig. 4). The increase of free InPc concentration to 30 μmol/L (results not shown) did not change significantly the results obtained using the concentration of 7.5 μmol/L. The ability of free zinc phthalocyanine (ZnPc) in reducing the viability of A549 cells was also not changed after concentration 17 μmol/L and the average viability was maintained at 62 % (Soares et al. 2011). Free ZnPc was not cytotoxic even using the concentration at 69 μmol/L (Soares et al. 2011). Probably the aggregate state of free InPc in the culture medium decreased the photodynamic efficiency of free InPc to reduce the cell viability (as will be shown later). The encapsulated InPc in PLGA-PEG nanoparticles or the free InPc was not cytotoxic for MCF-7 cells in the dark. The results shown that the InPc-loaded nanoparticles were more photocytotoxic than the free InPc since the cell viability was reduced from (82 ± 6) % (number of cells + free InPc + light) to (63 ± 3) % (number of cells + nano/InPc + light) when the InPc concentration was 3.8 μmol/L, and from (71 ± 8) % (number of cells + free InPc + light) to (47 ± 6) % (number of cells + nano/InPc + light) using the concentration 7.5 μmol/L (Fig. 4). This is in agreement with results obtained by other researchers who encapsulated photosensitizers into polymeric nanoparticles (Konan et al. 2003a; Zeisser-Labouebe et al. 2006). These results also revealed that free InPc photocytotoxicity was not dependent on the range of studied InPc concentration. Since the encapsulated and free InPc exhibit significant photocytotoxic effects at concentrations of 7.5 μmol/L in experiments with light, this concentration was used in subsequent assays.

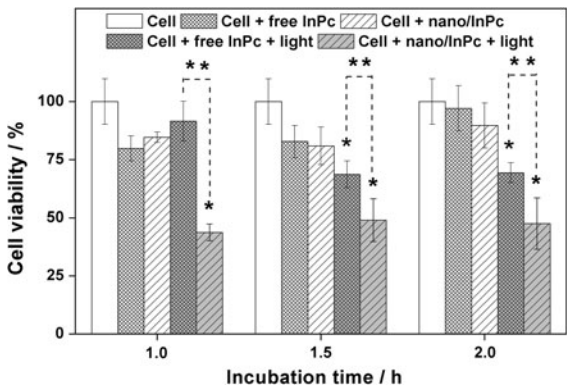

Fig. 3 Percent of cell viability versus incubation time on cytotoxicity (without light) and photocytotoxicity (with light) of InPc-loaded nanoparticles and free InPc. InPc concentration in InPc-loaded nanoparticles and in the aqueous cell culture media was 7.5 μmol/L. The MCF-7 cells were incubated with InPc-loaded nanoparticles and free InPc for different times (from 1 to 2 h) and then irradiated with a light dose of 7.5 J/cm^2 (light in figure legend) using a 665 nm laser diode with a power of 60 mW. The InPc-free nanoparticles, the source light and MP were not cytotoxic for cells (results not shown). Each data point is the mean ± SD of three values. (*) The differences of "cell" vs. "cell + nano/InPc + light", or "cell" vs. "cell + free InPc + light" or (**) "cell + free InPc + light" vs. "cell + nano/InPc + light" were significant at $p \leq 0.05$

Effect of laser power on InPc phototoxicity

The effectiveness of encapsulated InPc (Fig. 5) in causing cellular death was influenced by laser power since viability was reduced from (100 ± 9) % (number control of cells) to (64 ± 3) % (number of cells + nano/InPc + light) and then to (34 ± 3) %

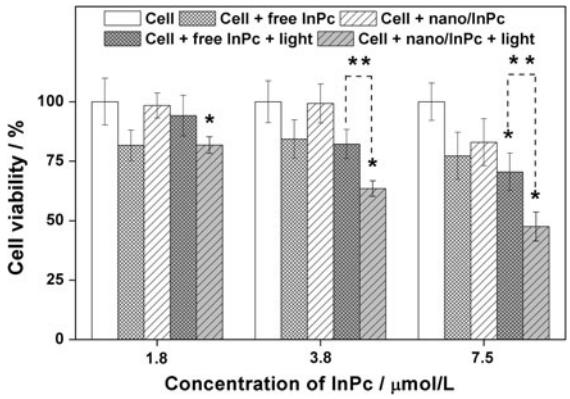

Fig. 4 Percent of cell viability versus InPc concentrations in InPc-loaded nanoparticles and in aqueous cell culture media on the cytotoxicity (without light) and photocytotoxicity (with light) of InPc-loaded nanoparticles and free InPc. MCF-7 cells were incubated with InPc-loaded nanoparticles or free InPc for 2 h and then irradiated with a light dose of 7.5 J/cm^2 (light, in figure legend) using a 665 nm diode laser with a power of 60 mW. The InPc-free nanoparticles, source light and MP were not cytotoxic for cells (results not shown). Each data point is the mean ± SD of three values. (*) The differences of "cell" vs. "cell + nano/InPc + light", or "cell" vs. "cell + free InPc + light" or (**) "cell + free InPc + light" vs. "cell + nano/InPc + light" were significant at $p \leq 0.05$

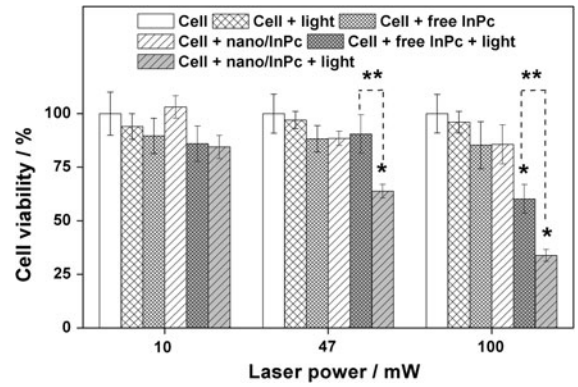

Fig. 5 Percent of cell viability versus laser power on cytotoxicity (without light) and photocytotoxicity (with light) of InPc-loaded nanoparticles and free InPc. InPc concentrations in InPc-loaded nanoparticles and in aqueous cell culture media was 7.5 μmol/L. MCF-7 cells were incubated with InPc-loaded nanoparticles or free InPc for 2 h and then irradiated using a 665 nm diode laser with different powers (10–100 mW) (light, in figure legend). The InPc-free nanoparticles and MP were not cytotoxic for cells (results not shown). Each data point is the mean ± SD of three values. (*)The differences of "cell" vs. "cell + nano/InPc + light", or "cell" vs. "cell + free InPc+ light" or (**) "cell + free InPc + light" vs. "cell + nano/InPc + light" were significant at $p \leq 0.05$

(number of cells + nano/InPc + light) when cells were incubated with InPc-loaded nanoparticles and irradiated with a laser power of 47 and 100 mW, respectively. The same dependence was not observed for free InPc when laser power was increased from 47 to 100 mW since viability was only reduced from (100 ± 9) % (number control of cells) to 60 ± 7 % when laser power was 100 mW (Fig. 5). Neither InPc-loaded nanoparticles nor free InPc caused the MCF-7 cell death when a laser power of 10 mW was used. The energy density emitted by laser was probably not efficient to observe the photodynamic effect when the laser power of 10 mW was used to excite the encapsulated InPc, or when laser power of 10–47 mW was used to excite the free InPc. Cells not incubated with free or encapsulated InPc were irradiated using different powers and no change was observed in the cell viability, indicating that the laser energy did not fried the MCF-7 cells. Results show clearly that the encapsulated InPc was more effective in causing the death of MCF-7 cells than free InPc since the cell viability was reduced from (90 ± 9) % (number of cells + free InPc + light) to (64 ± 3) % (number of cells + nano/InPc + light) when laser power was 47 mW, and from (60 ± 7) % (number of cells + free InPc + light) to (34 ± 3) % (number of cells + nano/InPc + light) when laser power was 100 mW (Fig. 5).

Localization and uptake of the encapsulated and free InPc into the MCF-7 cells

Figure 6 is the combination of four micrographies that relate InPc green fluorescence, DAPI blue fluorescence bound to the nucleus, phalloidin red fluorescence bound to the cytoskeleton, and a sum of these micrographies. InPc-loaded nanoparticles (Fig. 6a) as well as free InPc (Fig. 6b) were localized throughout the cytosol and in the perinuclear region, since the micrographs very clearly show the fluorescence emitted by InPc during excitation with a helium–neon laser. Micrographies also disclosed the presence of intense fluorescence of encapsulated InPc in the micro-region of the cytosol near the peripheral surface of the cell, suggesting the presence of aggregates of PLGA-PEG particles loaded with InPc inside and in the periphery of MCF-7 cells (Fig. 6a). The PLGA-PEG nanoparticles possess a highly hydrophilic surface coated with a PEG polymer. This characteristic could favor the interaction of nanoparticles with the

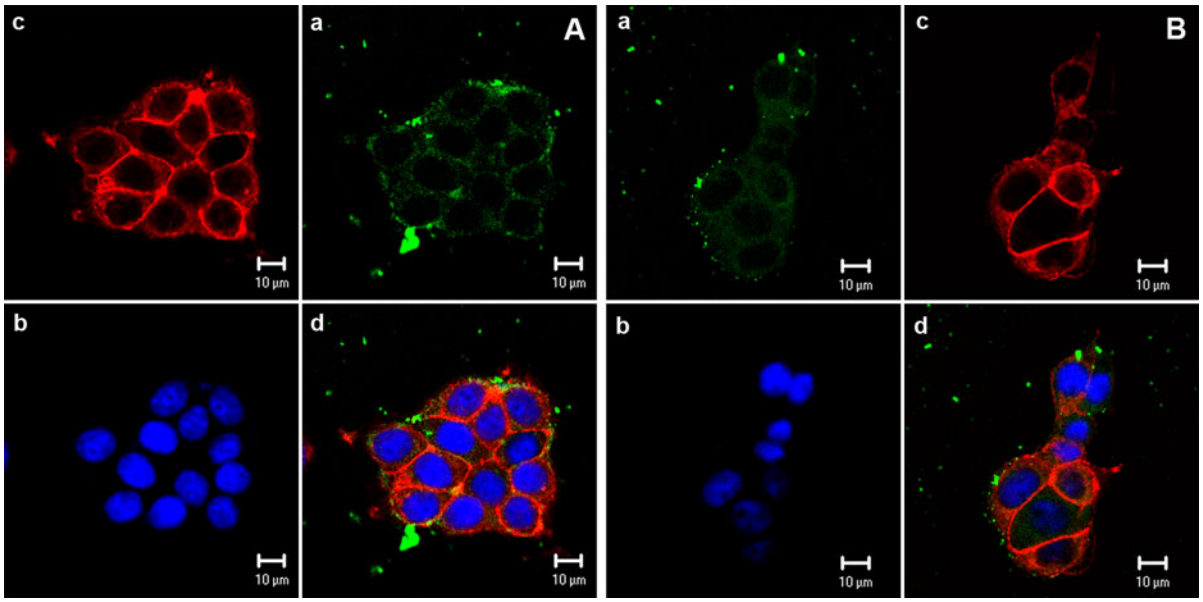

Fig. 6 Confocal micrographs of MCF-7 cells incubated for 2 h with 7.5 µmol/L of **a** InPc encapsulated into nanoparticles or **b** free InPc. (*a*) InPc green fluorescence (helium–neon laser, $\lambda_{ex} = 633$ nm); (*b*) DAPI blue fluorescence (mercury lamp, $\lambda_{ex} = 365$–372 nm) bound to DNA for staining the nucleus; (*c*) Phalloidin red fluorescence (argon laser $\lambda_{ex} = 543$ nm) bound to F-actin for staining the cytoskeleton and (*d*) a sum of the three earlier micrographies. Similar results were obtained with the other nanoparticle formulations and free InPc (results not shown)

hydrophilic external membrane of the cell, causing a concentration of PLGA-PEG nanoparticles in the peripheral area of the cell. However, intense fluorescence was also detected in the region away from the surface of the cell. Therefore, it was evaluated if the aggregation could be caused due to the interaction between culture medium and nanoparticles. The average size was measured at determined period during the incubation of nanoparticles only with culture medium for 2 h. One population of nanoparticles [(98 ± 2) %] with an average size of (132 ± 2) nm and other population [(2 ± 1) %] with an average size of (383 ± 13) nm were observed after 0.33 h of incubation, suggesting that the nanoparticle aggregates were generated in the culture medium (Fig. 7a). Large particles were not observed for incubation time smaller than 0.33 h.

The nanoparticle aggregates increased during the incubation time since the population of large particles increased from 0 to (6 ± 1) % and the population of small particles decreased from (100 ± 3) to (94 ± 1) % after 2 h of incubation with the culture medium, while the average size of large particles increased from 0 to (1579 ± 16) nm and the small particles increased from (128 ± 10) to (151 ± 12) nm (Fig. 7a). Experiments were also performed with water instead culture medium to evaluate if the aggregates were generated by interaction of nanoparticles with the culture medium (Fig. 7b). The results disclosed that the population of large aggregates of particles [(20 ± 2) %] was bigger in water than that obtained in the culture medium [(6 ± 1) %] after 2 h of incubation, as well as the size was also larger since the average size of aggregates was (5950 ± 66) nm while in the culture medium the average size was (1579 ± 16) nm (Fig. 7). The presence of non-ionic surfactant reduced the population and the size of the aggregates since the average size was reduced from (5950 ± 66) to (778 ± 17) nm and from (1579 ± 16) to (1155 ± 17) nm when Tween® 20 (0.24 mmol/L) was added in water and in medium culture, respectively. This result allows hypothesizing that the culture medium helped to reduce the aggregates of InPc-loaded nanoparticles. Probably, the aggregates of nanoparticles observed in the medium culture and in the confocal micrographies were generated due to the nanoparticles concentration used in the experiments because of the small loading of the InPc into the nanoparticles. Unfortunately, the better values for loading were not possible because of the diffusion of

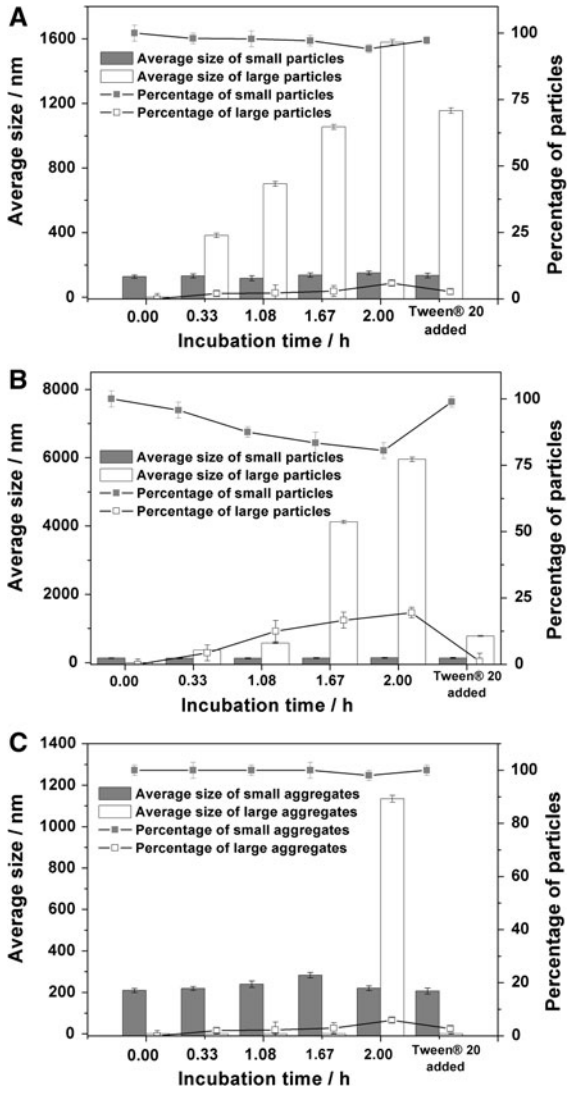

Fig. 7 Average size and percentage of InPc-loaded PLGA-PEG nanoparticles incubated with **a** the culture medium and **b** water. Nanoparticles were incubated from 0 to 2 h and the average size and percentage of particles were measured in a predetermined time. **c** Average size and percentage of aggregates of the free InPc incubated with culture medium was also measured. After 2.0 h of incubation, a Tween® 20 solution (0.24 mmol/L) was added to the nanoparticle or the free InPc solutions and the size and percentage of particles were measured again. Each data point is the mean ± SD of three values

the InPc for the aqueous phase due to the interaction with ethanol and PVA (results will be published).

Similarly, an intense fluorescence of free InPc aggregates was localized in the peripheral region of MCF-7 cells (Fig. 6b), suggesting that free InPc aggregates could be localized on the surface of cells. Studies have shown that hydrophobic photosensitizers tend to be localized in cytoplasmatic membrane (Moor 2000; Ochsner 1997). However, the intense fluorescence of free InPc was also detected in regions away from of the cell. The free InPc solution in the culture medium was also monitored by dynamic light scattering to evaluate the presence of aggregates. Theoretically, free InPc aggregates should not be detected if the solution was homogenous, but when free InPc solution prepared in MP was diluted in the culture medium, the aggregates were detected in initial of the experiment (Fig. 7c). The average size of small aggregates increased from (209 ± 10) to (283 ± 13) nm after 1.67 h of incubation. One population [(1.9 ± 1) %] of large aggregates were detected after 2.0 h. However, the large aggregates were eliminated when Tween® 20 (0.24 mmol/L) was added in medium culture suggesting that the large aggregates were reduced to smaller size. These results suggest that the molecules of free InPc aggregated in culture medium due to the hydrophobicity of InPc (as will be shown later). Therefore, the intense fluorescence detected outside of the cell was emitted by aggregates of free InPc.

Fluorescence from InPc-loaded nanoparticles or free InPc within the nucleus was not observed. Thus, there is no risk of photocarcinogenesis for surviving cells (Berg et al. 1990).

Cells incubated with nanoparticles of PLGA-PEG without entrapped InPc did not present fluorescence (not shown), confirming that the fluorescence observed for nanoparticles loaded with InPc is only due to the photosensitizer. The fluorescence intensity of internalized InPc-loaded nanoparticles was higher than that of the free InPc, suggesting that a greater amount of encapsulated InPc was internalized in the cells in comparison with free InPc. This hypothesis was evaluated by a quantification of the amount of encapsulated and free InPc internalized in the cells. Although the results have corroborated the confocal micrographs (not shown), it was not possible to consider the quantification of the amount of encapsulated and the free InPc into the cells since the nanoparticle aggregates and free InPc aggregates were not eliminated when the cells were rinsed with phosphate-buffered saline solution. Probably the results reflected the amount of encapsulated and free InPc localized inside and outside of the cell. Studies have shown that the encapsulation of photosensitizers can enhance the amount of internalized

photosensitizer in the cell, a fact that will depend on the photosensitizer, the carrier used in encapsulation and the cell line studied (Nishiyama et al. 2009; Konan et al. 2003b). The encapsulation of InPc and the low solubility of free InPc in the culture medium explain the greater efficiency of encapsulated InPc in reducing MCF-7 cell viability than free InPc.

Optical cross-sections were obtained from the top of the cells, with a gradual increase of 1.57 and 0.79 μm in depth, respectively, for cells incubated with InPc-loaded nanoparticles or with free InPc to evaluate if encapsulated or free InPc were distributed within cells and/or near the cell surface. Figure 8a confirmed the presence of InPc-loaded nanoparticles inside MCF-7 cells since the fluorescence persisted in all optical sections (Fig. 8a). However, the distribution of InPc-loaded nanoparticles in the cells was not homogeneous since the fluorescence intensity from nanoparticles was not uniform within these optical sections. Similar results were observed for the distribution of free InPc into the MCF-7 cell (Fig. 8b). But, the intensity of green fluorescence from free InPc within the optical sections was smaller than that emitted by InPc-loaded nanoparticle, corroborating with results obtained in Fig. 6.

Hydrophobic photosensitizers tend to aggregate in cell culture media due to the susceptibility of the hydrophobic skeleton to avoid contact with water molecules (Rosenthal 1991). The aggregation state hinders the efficacy of InPc by decreasing its bioavailability and limiting its capacity to absorb light (Bechet et al. 2008; Juzeniene et al. 2006). The

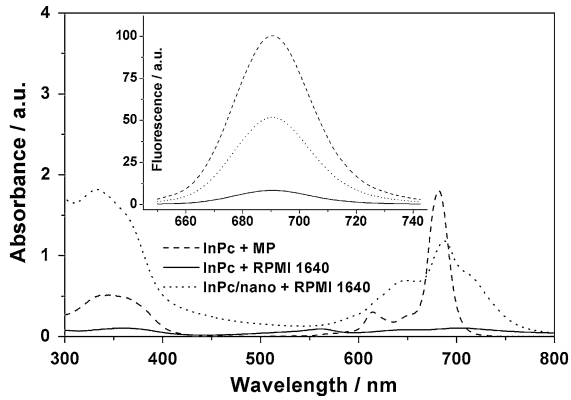

Fig. 9 Free and encapsulated InPc absorbance and (*inset*) fluorescence spectra at a concentration of 7.5 μmol/L in RPMI 1640 medium. Free InPc absorbance spectrum was also obtained in the same concentration but in MP. InPc was excited at 620 nm in both solutions

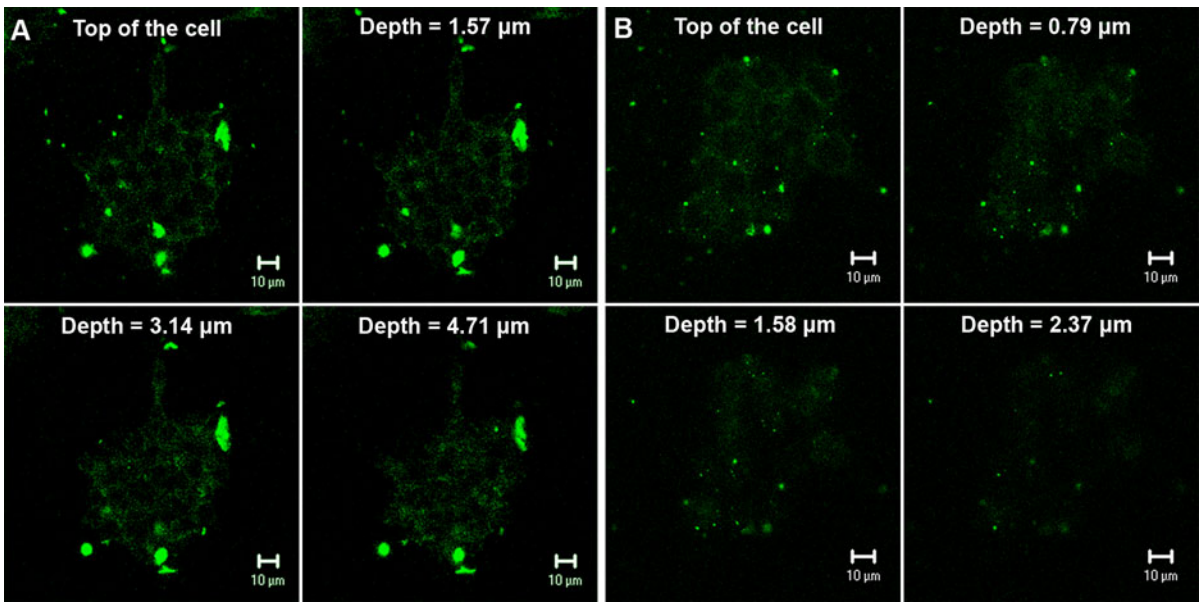

Fig. 8 Confocal micrographs of optical cross-sections taken with a gradual increase of 1.57 and 0.79 μm in depth from the top of the cell (*top row*) after incubation with **a** InPc-loaded nanoparticles or **b** free InPc (7.5 μmol/L) for 2 h. InPc was excited with a helium–neon laser ($\lambda_{ex} = 633$ nm)

aggregation of free InPc in an RPMI 1640 medium was also evaluated by absorbance and fluorescence measurements (Fig. 9). The absorbance spectrum of free InPc in an RPMI 1640 medium, compared with that obtained in MP, suggested that the InPc is aggregated in the culture medium since the wavelength of maximum absorbance of free InPc was red shifted by 20 nm in the RPMI medium, with a concomitant decrease in absorbance intensity and a broadening of the Q band (400–800 nm) (Fig. 9), corroborating with results obtained in Fig. 7c. The molar absorptivity of the photosensitizer decreases significantly when large self-associated supra-structures are formed, causing a decrease in absorbance intensity and, consequently, a reduction in the free InPc capability to absorb incident radiation (Reddi and Jori 1988). These large aggregates can also scatter incident radiation favoring a reduction in the absorption of free InPc. The InPc fluorescence also decreased (Fig. 9, inset) in the RPMI medium, in comparison with the spectrum intensity in MP. The aggregates have a reduced tendency for crossing plasmatic membranes and consequently have lower cellular uptake. Thus, lower effectiveness of free InPc in causing MCF-7 cell death can be associated to the lipophilic character of InPc, which favors the aggregation state in the aqueous culture medium. This reduces the capability of InPc to absorb incident radiation and decreases its cellular uptake, and its subsequent ability to produce singlet oxygen.

The absorbance and fluorescence spectra of the encapsulated InPc, compared with that obtained in MP, also suggested the presence of aggregates of photosensitizer in the culture medium since the absorbance and fluorescence intensities decreased and Q band suffered a broadening. However, the absorbance and fluorescence intensities of encapsulated InPc were higher than that obtained to the free InPc. Especially, for absorbance spectrum of encapsulated InPc, the wavelengths considered in the conclusion were between 600–800 nm since wavelengths smaller than 600 nm presented higher scattering, causing an exponential profile in the spectrum. It is known that scattering is more intense in regions of smaller wavelength since the scattering intensity (SI) is inversely proportional to the wavelength raised to the fourth power ($SI \propto 1/\lambda^4$) (Li et al. 2000). These results suggest that the aggregation of the encapsulated InPc was smaller than that the free InPc.

Generation of singlet oxygen by encapsulated and free InPc

The capacity of encapsulated and free InPc in generating singlet oxygen was monitored by EPR measurements using TEMP as a singlet oxygen trapping agent (Lion et al. 1976; Shutova et al 2000). The irradiation of the culture medium containing nanoparticles loaded with InPc led to the generation of an EPR signal (Fig. 10a). The triplet EPR signal is characteristic of a stable nitroxide radical (TEMPONE) resulting from the reaction between singlet oxygen and TEMP (Lion et al. 1976; Xu et al. 2003). The EPR signals increased gradually with the increase in incident light from 3 to 7.5 J/cm^2, suggesting that singlet oxygen was generated. This result is important because it shows the ability of encapsulated InPc to interact with molecular oxygen and that PLGA-PEG does not act as an impermeable barrier. Before irradiation of TEMP, a small signal was detected due to the presence of TEMPONE impurities.

The EPR signal did not change with an increase in the light dose when the culture medium was irradiated in the presence of free InPc (Fig. 10b). Experiments were performed in the presence of a non-ionic surfactant to evaluate the importance of aggregation on generating singlet oxygen. The free InPc generated singlet oxygen in the presence of Tween® 20 (Fig. 10c) suggesting that the photosensitizer aggregation reduced the efficacy of free InPc in generating singlet oxygen, and consequently the effectiveness in decreasing the viability of MCF-7 cells. This result corroborates with the decrease in absorbance and fluorescence intensity of the free InPc spectrum.

A similar experiment performed with InPc-loaded nanoparticles and Tween® 20 caused an increase in EPR signal intensity (Fig. 10d) suggesting the molecules adsorbed in the surface of nanoparticles could be released into the culture medium in the presence of a surfactant. Besides, InPc molecules adsorbed on the nanoparticles surface could be responsible for the photodynamic effect of the encapsulated photosensitizer on the death of MCF-7 cells. To evaluate this hypothesis, we incubated the InPc-loaded nanoparticles with TEMP solution for 30 min. Before irradiation, the suspension was centrifuged and the nanoparticles were discarded. The results revealed that InPc-loaded nanoparticles were important for the generation of singlet oxygen since the EPR signal was

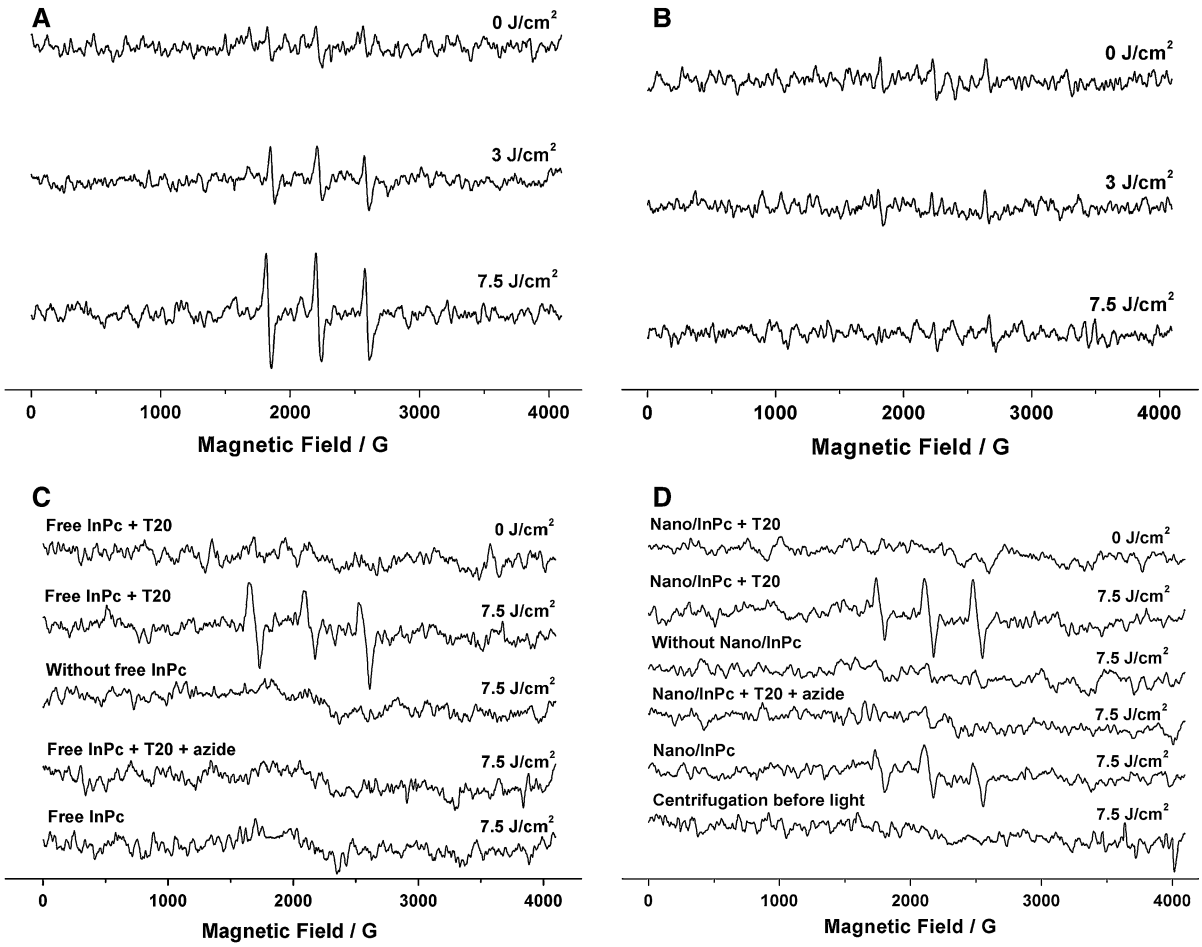

Fig. 10 EPR spectra of TEMPONE generated by photooxidation of 2,2,6,6-tetramethylpiperidone (23 mmol/L) at room temperature (25 °C) in the presence of **a** encapsulated and **b** free InPc (7.5 μmol/L), in an RPMI 1640 culture medium. The generation of TEMPONE signal by **c** free and **d** encapsulated InPc was also monitored in the presence of 0.24 mmol/L of Tween® 20 and 5.0 μ mol/L of azide (singlet oxygen quencher). For assessing whether singlet oxygen is generated by encapsulated InPc or by InPc molecules that were released from nanoparticles into the culture medium, the nanoparticles were incubated for 30 min in the medium and after this time, the medium was centrifuged before irradiation. Light source: laser diode 665 nm. Light doses of 7.5 J/cm^2 and laser power of 100 mW were used in this experiment

not observed after the discarding of nanoparticles before the light dose. The Tween® 20 probably reduced the nanoparticle aggregates, favoring photodynamic action of the greater amount of InPc-loaded nanoparticles, increasing the EPR signal.

An experiment performed in the presence of azide (a quencher of singlet oxygen) did not show the triplet EPR pattern for the encapsulated or the free InPc, corroborating that the photodynamic effect was caused by a generation of singlet oxygen. Control irradiations of only the culture medium or the free InPc in water were carried out and no changes were observed (results not shown).

Studies of free and encapsulated InPc photobleaching

Phthalocyanines have the tendency to suffer photobleaching (Bonnett and Martinez 2001). Thus, it is possible that InPc photobleaching reduces the photodynamic efficacy of free and encapsulated InPc in decreasing the MCF-7 cell viability or generating the EPR signal. For evaluating whether the encapsulated and free InPc suffer photobleaching during the irradiation and whether the encapsulation decreases the photobleaching of the photosensitizer, we monitored the absorbance spectrum of free and encapsulated InPc

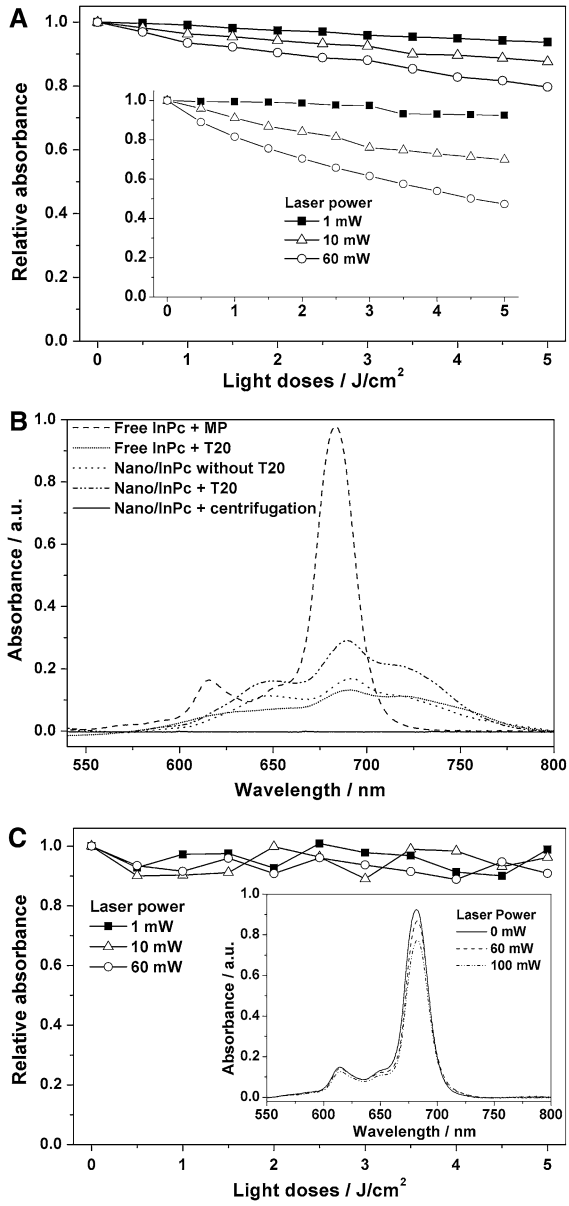

Fig. 11 Free InPc photobleaching in **a** PBS solution and (*inset*) in organic solvent. The decrease in relative absorbance of InPc solution with concentration of 5.0 μmol/L was monitored at 682 nm for the free InPc solubilized in MP, and at 690 nm for the PBS solution containing the free InPc and 0.24 mmol/L of Tween® 20. The solutions were irradiated with light doses from 0.5 to 5.0 J/cm^2 and laser power from 1 to 60 mW, using a laser diode 665 nm. **b** Absorption spectra of free InPc (5.0 μmol/L) in MP and in PBS solution with Tween® 20, and of encapsulated InPc (5.0 μmol/L) in PBS solution with and without Tween® 20. The encapsulated InPc spectrum was also measured after centrifugation of the suspension for discarding the nanoparticles loaded with InPc. **c** The photobleaching of encapsulated InPc was also monitored in the PBS solution. (**c**, *inset*) Absorbance spectra of InPc-loaded nanoparticles (InPc concentration of 5.0 μmol/L) dissolved in MP before and after irradiation with a light dose of 5 J/cm^2 and a laser power of 60 and 100 mW. After the light dose, the suspension of InPc-loaded nanoparticles in PBS solution was centrifuged at 20,400×*g* for 20 min, the supernatant was discarded and the nanoparticles were dissolved with MP

during light doses (Fig. 11). It is known that the RPMI 1640 medium is a mixture of enriched salts with amino acids, vitamins, glucose and glutathione. We showed that RPMI 1640 can reduce the photobleaching of photosensitizers because some constituents of the culture medium quenched the singlet oxygen (Silva et al. 2009). Thus, we decided to study InPc photobleaching in a PBS solution to prevent the influence of the culture medium on the experiment results.

The results show that the relative absorbance intensity of free InPc (Fig. 11a), solubilized in PBS solution and Tween® 20, decreases from 1.0 to 0.8 with the increase in incident light from 0 to 5 J/cm^2 using a laser power of 60 mW. A smaller reduction in relative absorbance intensity was obtained when the laser power was 1 and 10 mW than when using a power of 60 mW. After a light dose of 5 J/cm^2 the relative absorbance intensity was reduced from 0.94 to 0.88 (Fig. 11a) when the laser power was increased from 1 to 10 mW, and then to 0.80 when the laser power was 60 mW. These results suggest that the free InPc was photobleached during the light doses. Free InPc dissolved in MP (an organic solvent), irradiated with the same light doses and the same laser powers, revealed higher photobleaching (Fig. 11a, inset) than what was observed for free InPc in PBS solution (Fig. 11a) since after a light dose of 5 J/cm^2 the relative absorbance intensity of free InPc in organic solvent was reduced from 0.93 to 0.47 when the laser power was increased from 1 to 60 mW. The aggregation state of the free InPc in PBS solution was corroborated by an InPc absorbance spectrum characterized by a large Q band with small absorbance intensity (Fig. 11b). Thus, the aggregation state of free InPc favors a decrease in InPc photobleaching.

The results of the encapsulated InPc photobleaching were inconclusive since relative absorbance intensity decreased and increased using the same light doses and the same laser power as used for experiments with free InPc (Fig. 11c). Probably, the light scattered by nanoparticles in PBS solution hampered

the measurements of absorbance. These results could suggest that the encapsulated InPc was not photobleached. This hypothesis was evaluated measuring the InPc absorbance spectrum after light dose on the nanoparticle solution, subsequent centrifugation of the nanoparticle suspension, discarding of the supernatant, and dissolution of the InPc-loaded nanoparticles in MP. The intensity of the absorbance spectrum obtained by dissolving the InPc-loaded nanoparticles in MP decreased after irradiation with a light dose of 5.0 J/cm^2 and a laser power of 60 and of 100 mW (Fig. 11c, inset). This is an indication that encapsulated InPc was photobleached and that the oxygen can interact with the photosensitizer encapsulated in the nanoparticle. This outcome corroborates with EPR results since encapsulation is not a barrier for photobleaching or for generating singlet oxygen. Figure 11c (inset) disclosed that the decrease in InPc absorbance intensity was smaller for encapsulated InPc than observed for free InPc using the same light dose and laser power, since the relative absorbance of free InPc after a light dose of 5 J/cm^2 and a laser power of 60 mW was reduced from 1 (integral absorbance intensity) to 0.79 (a decrease of 20 % in InPc absorbance intensity) (Fig. 11a) while the relative absorbance of encapsulated InPc was reduced from 1 to 0.93 (a decrease of 7 % in InPc absorbance intensity) (Fig. 11c, inset). Even a laser power of 100 mW reduced the relative absorbance of encapsulated InPc from 1 to 0.86 (a decrease of 14 % in InPc absorbance intensity) (Fig. 11c, inset).

Absorbance measurement was also performed for encapsulated InPc in a PBS solution with and without surfactant before the light doses (Fig. 11b). The absorbance intensity of the encapsulated InPc spectrum was higher in PBS solutions with surfactant than that measured without Tween® 20. After centrifugation of the PBS solution containing the encapsulated InPc for discarding the nanoparticles, the InPc absorbance signal was quenched. Thus, the results suggest the surfactant must reduce the aggregation of nanoparticles increasing the InPc absorbance signal, corroborating with results shown in Fig. 7a, b, and that the increase in signal is not due to InPc molecules adsorbed in the surface of nanoparticles that could be released in the PBS solution. This is corroborating with an increase in the EPR signal when TEMP was irradiated in the presence of InPc-loaded nanoparticles and Tween® 20 (Fig. 10d).

Therefore, encapsulated InPc suffers less photobleaching than free InPc, which favors better photodynamic efficiency for encapsulated InPc in generating the EPR signal. The photobleaching of free InPc and its aggregation state in the culture medium probably reduces the efficacy of the free photosensitizer for causing tumor cell death.

Conclusion

This study demonstrated that the encapsulation of InPc into PLGA-PEG nanoparticles improves the photobiological and photodynamic activity of the photosensitizer. The photocytotoxicity of encapsulated InPc was observed after 1 h of incubation with MCF-7 cells, and was depended on photosensitizer concentration and laser power. The same result was not observed for free InPc. InPc-loaded nanoparticles were more effective than free InPc in inducing MCF-7 cell death. The increase in phototoxicity of InPc-loaded nanoparticles was related to the low solubility of free InPc in the culture medium. The aggregation state and the photobleaching of free InPc reduce both cellular uptake and its ability to produce singlet oxygen. Encapsulation is not a barrier to InPc for generating singlet oxygen. Moreover, encapsulation decreases the photobleaching of InPc, favoring the augmentation of their photocytotoxicity.

Acknowledgments We thank the Conselho Nacional de Desenvolvimento Científico e Tecnológico (CNPq) and the Federal Institute of Espírito Santo for financial support, the Instituto Nacional de Ciência e Tecnologia de Fotônica Aplicada à Biologia Celular (INFABIC) for the confocal microscopy analysis and Prof. Geovane Lopes de Sena from Federal University of Espírito Santo for fluorescence analysis.

References

Acharya S, Sahoo SK (2011) PLGA nanoparticles containing various anticancer agents and tumor delivery by EPR effect. Adv Drug Deliv Rev 63:170–183. doi:10.1016/j.addr.2010.10.008

Allison RR, Mota HC, Bagnato VS, Sibata CH (2008) Bionanotechnology and photodynamic therapy. State of the art review. Photodiagn Photodyn Ther 5:19–28. doi:10.1016/j.pdpdt.2008.02.001

Bechet D, Couleaud P, Frochot C, Viriot ML, Guillemin F, Barberi-Heyob M (2008) Nanoparticles as vehicles for delivery of photodynamic therapy agents. Trends Biotechnol 26:612–621. doi:10.1016/j.tibtech.2008.07.007

Berg K, Western A, Bommer JC, Moan J (1990) Intracellular localization of sulfonated mesotetraphenylporphines in a human carcinoma cell line. Photochem Photobiol 52:481–487. doi:10.1111/j.1751-1097.1990.tb01789.x

Blander JM, Medzhitov R (2006) Toll-dependent selection of microbial antigens for presentation by dendritic cells. Nature 440:808–812. doi:10.1038/nature04596

Bonnett R, Martinez G (2001) Photobleaching of sensitizers used in photodynamic therapy. Tetrahedron 57:9513–9547. doi:10.1016/S0040-4020(01)00952-8

Bourdon O, Mosqueira V, Legrand P, Blais J (2000) A comparative study of the cellular uptake, localization and phototoxicity of meta-tetra(hydroxyphenyl) chlorin encapsulated in surface-modified submicronic oil/water carriers in HT29 tumor cells. J Photochem Photobiol B 55:164–171. doi:10.1016/S1011-1344(00)00043-9

Bozzini G, Collin P, Betrouni N, Nevoux P, Ouzanne A, Puech P, Villers A, Mordon S (2012) Photodynamic therapy in urology: what can we do now and where are we heading? Photodiagn Photodyn Ther 9:261–273. doi:10.1016/j.pdpdt.2012.01.005

Calzavara-Pinton PG, Venturini M, Sala R (2005) A comprehensive overview of photodynamic therapy in the treatment of superficial fungal infections of the skin. J Photochem Photobiol B 78:1–6. doi:10.1016/j.jphotobiol.2004.06.006

Chen Y, Zheng X, Dobhal MP, Gryshuk A, Morgan J, Dougherty TJ, Oseroff A, Pandey RK (2005) Methyl pyropheophorbide-a analogs: potential fluorescent probes for the peripheral-type benzodiazepine receptor. Effect of central metal in photosensitizing efficacy. J Med Chem 48:3692–3695. doi:10.1021/jm050039k

Cruz LJ, Tacken PJ, Fokkink R, Figdor CG (2011) The influence of PEG chain length and targeting moiety on antibody-mediated delivery of nanoparticle vaccines to human dendritic cells. Biomaterials 32:6791–6803. doi:10.1016/j.biomaterials.2011.04.082

Garcia AM, Alarcon E, Munoz M, Scaiano JC, Edwards AM, Lissi E (2011) Photophysical behavior and photodynamic activity of zinc phthalocyanines associated to liposomes. Photochem Photobiol Sci 10:507–514. doi:10.1039/c0pp00289e

Gref R, Minamitake Y, Peracchia MT, Trubetskoy V, Torchilin V, Langer R (1994) Biodegradable long-circulating polymeric nanospheres. Science 263:1600–1603. doi:10.1126/science.8128245

Hans ML, Lowman AM (2002) Biodegradable nanoparticles for drug delivery and targeting. Curr Opin Solid State Mater Sci 6:319–327. doi:10.1016/S1359-0286(02)00117-1

Jeffery H, Davis SS, O'Hagan DT (1991) The preparation and characterization of poly(lactide-co-glycolide) microparticles, I. Oil-in-water emulsion solvent evaporation Int J Pharm 77:169–175. doi:10.1016/0378-5173(91)90314-E

Jokerst JV, Lobovkina T, Zare RN, Gambhir SS (2011) Nanoparticle PEGylation for imaging and therapy. Nanomed 6:715–728. doi:10.2217/nnm.11.19

Juzeniene A, Nielsen KP, Moan J (2006) Biophysical aspects of photodynamic therapy. J Environ Pathol Toxicol Oncol 25:7–28. doi:10.1615/JEnvironPatholToxicolOncol.v25.i1-2.20

Kamaly N, Xiao Z, Valencia PM, Radovic-Moreno AF, Farokhzad OC (2012) Targeted polymeric therapeutic nanoparticles: design, development and clinical translation. Chem Soc Rev 41:2971–3010. doi:10.1039/c2cs15344k

Knop K, Hoogenboom R, Fischer D, Schubert US (2010) Poly(ethylene glycol) in drug delivery: pros and cons as well as potential alternatives. Angew Chem Int Ed 49:6288–6308. doi:10.1002/anie.200902672

Konan YN, Gurny R, Allemann E (2002) State of the art in the delivery of photosensitizers for photodynamic therapy. J Photochem Photobiol B 66:89–106. doi:10.1016/S1011-1344(01)00267-6

Konan YN, Berton M, Gurny R, Allemann E (2003a) Enhanced photodynamic activity of meso-tetra(4-hydroxyphenyl)porphyrin by incorporation into sub-200 nm nanoparticles. Eur J Pharm Sci 18:241–249. doi:10.1016/S0928-0987(03)00017-4

Konan YN, Chevallier J, Gurny R, Allemann E (2003b) Encapsulation of p-THPP into nanoparticles: cellular uptake, subcellular localization and effect of serum on photodynamic therapy. Photochem Photobiol 77:638–644. doi:10.1562/0031-8655(2003)0770638EOPINC2.0.CO2

Korbelik M, Madiyalakan R, Woo T, Haddadi A (2012) Antitumor efficacy of photodynamic therapy using novel nanoformulations of hypocrellin photosensitizer SL052. Photochem Photobiol 88:188–193. doi:10.1111/j.1751-1097.2011.01035.x

Li K, Ma CQ, Liu Y, Zhao FL, Tong SY (2000) Rayleigh light scattering and its applications to biochemical analysis. Chin Sci Bull 45:386–394. doi:10.1007/10.1007/BF02884935

Lion Y, Delmelle M, van de Vorst A (1976) New method of detecting singlet oxygen production. Nature 263:442–443. doi:10.1038/263442a0

Lochmann A, Nitzsche H, von Einem S, Schwarz E, Mader K (2010) The influence of covalently linked and free polyethylene glycol on the structural and release properties of rhBMP-2 loaded microspheres. J Control Release 147:92–100. doi:10.1016/j.jconrel.2010.06.021

Maeda H, Wu J, Sawa T, Matsumura Y, Hori K (2000) Tumor vascular permeability and the EPR effect in macromolecular therapeutics: a review. J Control Release 65:271–284. doi:10.1016/S0168-3659(99)00248-5

Moor ACE (2000) Signaling pathways in cell death and survival after photodynamic therapy. J Photochem Photobiol B 57:1–13. doi:10.1016/S1011-1344(00)00065-8

Mundargi RC, Babu VR, Rangaswamy V, Patel P, Aminabhavi TM (2008) Nano/micro technologies for delivering macromolecular therapeutics using poly(D, L-lactide-co-glycolide) and its derivatives. J Control Release 125:193–209. doi:10.1016/j.jconrel.2007.09.013

Nishiyama N, Nakagishi Y, Morimoto Y, Lai P, Miyazaki K, Urano K, Horie S, Kumagai M, Fukushima S, Cheng Y, Jang W, Kikuchi M, Kataoka K (2009) Enhanced photodynamic cancer treatment by supramolecular nanocarriers charged with dendrimer phthalocyanine. J Control Release 133:245–251. doi:10.1016/j.jconrel.2008.10.010

O'Connor AE, Gallagher WM, Byrne AT (2009) Porphyrin and nonporphyrin photosensitizers in oncology: preclinical and clinical advances in photodynamic therapy. Photochem Photobiol 85:1053–1074. doi:10.1111/j.1751-1097.2009.00585.x

Ochsner M (1997) Photophysical and photobiological processes in the photodynamic therapy of tumours. J Photochem Photobiol B 39:1–18. doi:10.1016/S1011-1344(96)07428-3

Qiang YG, Zhang XP, Li J, Huang Z (2006) Photodynamic therapy for malignant and non-malignant diseases: clinical investigation and application. Chin Med J 119: 845–857

Reddi E, Jori G (1988) Steady-state and time-resolved spectroscopic studies of photodynamic sensitizers: porphyrins and phthalocyanines. Rev Chem Intermed 10:241–268. doi:10.1007/BF03155995

Rosenfeld A, Morgan J, Goswami LN, Ohulchankyy T, Zheng X, Prasad PN, Oseroff A, Pandey RK (2006) Photosensitizers derived from 13^2-oxo-methyl pyropheophorbide-a: enhanced effect of indium(III) as a central metal in vitro and in vivo photosensitizing efficacy. Photochem Photobiol 82:626–634. doi:10.1562/2005-09-29-RA-704

Rosenthal I (1991) Phthalocyanines as photodynamic sensitizers. Photochem Photobiol 53:859–870

Sekkat N, van den Bergh H, Nyokong T, Lange N (2012) Like a bolt from the blue: phthalocyanines in biomedical optics. Molecules 17:98–144. doi:10.3390/molecules17010098

Sharma SK, Mroz P, Daí T, Huang Y, Denis TGS, Hamblin MR (2012) Photodynamic therapy for cancer and for infections: what is the difference? Israel J Chem 52:691–705. doi:10.1002/ijch.201100062

Shutova T, Kriska T, Nemeth A, Agabekov V, Gal D (2000) Physicochemical modeling of the role of free radicals in photodynamic therapy. Biochem Biophys Res Commun 270:125–130. doi:10.1006/bbrc.2000.2385

Silva AR, Inada NM, Rettori D, Baratti MO, Vercesi AE, Jorge RA (2009) In vitro photodynamic activity of chloro (5,10,15,20-tetraphenylporphyrinato)indium(III) loaded-poly(lactide-co-glycolide) nanoparticles in LNCaP prostate tumour cells. J Photochem Photobiol B 94:101–112. doi:10.1016/j.jphotobiol.2008.10.010

Silva AR, de Oliveira AM, Augusto F, Jorge RA (2011) Effects of preparation conditions on the characteristics of PLGA nanospheres loaded with chloro(5,10,15,20-tetraphenylporphyrinato)indium(III). J Nanosci Nanotechnol 11:5234–5246. doi:10.1166/jnn.2011.4136

Soares MV, Oliveira MR, dos Santos EP, Gitirana LB, Barbosa GM, Quaresma CH, Ricci-junior E (2011) Nanostructured delivery system for zinc phthalocyanine: preparation, characterization, and phototoxicity study against human lung adenocarcinoma A549 cells. Int J Nanomed 6:227–238. doi:10.2147/IJN.S15860

Stillman MJ, Nyokong T (1989) Chemical fixation and photoreduction of carbon dioxide catalyzed by metal phthalocyanine derivatives. In: Leznoff CC, Lever ABP (eds) Phthalocyanines: properties and applications, vol 1. chapter 3. Wiley, New York

Triesscheijn M, Baas P, Schellens JHM, Stewart FA (2006) Photodynamic therapy in oncology. Oncol 11:1034–1044. doi:10.1634/theoncologist.11-9-1034

Win KY, Feng SS (2005) Effects of particle size and surface coating on cellular uptake of polymeric nanoparticles for oral delivery of anticancer drugs. Biomaterials 26:2713–2722. doi:10.1016/j.biomaterials.2004.07.050

Xu S, Chen S, Zhang M, Shen T (2003) Synthesis, characterization and photodynamic activity of phenmethylamino-demethoxy-hypocrellin B. J Photochem Photobiol B 72:61–67. doi:10.1016/j.jphotobiol.2003.09.001

Zeisser-Labouebe M, Lange N, Gurny R, Delie F (2006) Hypericin-loaded nanoparticles for the photodynamic treatment of ovarian cancer. Int J Pharm 326:174–181. doi:10.1016/j.ijpharm.2006.07.012